The skin is a significant but overlooked anatomical reservoir for vector-borne African trypanosomes

Paul Capewell, Christelle Cren-Travaillé, Francesco Marchesi, Pamela Johnston, Taylor-Anne Gorman, Estefania Calvo-Alvarez, Aline Crouzols, Grégory Jouvion, Vincent Jammoneau, William Weir, et al.

The skin is a significant but overlooked anatomical reservoir for vector-borne African trypanosomes

Paul Capewell[1*], Christelle Cren-Travaillé[2*], Francesco Marchesi[3], Pamela Johnston[3], Caroline Clucas[1], Robert A Benson[4], Taylor-Anne Gorman[1,4], Estefania Calvo-Alvarez[2], Aline Crouzols[2], Grégory Jouvion[5], Vincent Jammoneau[6], William Weir[1], M Lynn Stevenson[3], Kerry O'Neill[1], Anneli Cooper[1], Nono-raymond Kuispond Swar[7], Bruno Bucheton[6], Dieudonné Mumba Ngoyi[8], Paul Garside[4], Brice Rotureau[2**] and Annette MacLeod[1**]

[1]Wellcome Trust Centre for Molecular Parasitology, College of Medical, Veterinary and Life Sciences, Henry Wellcome Building for Comparative Medical Sciences, Garscube Estate, Glasgow, United Kingdom, G61 1QH

[2]Trypanosome Transmission Group. Trypanosome Cell Biology Unit, INSERM U1201 & Department of Parasites and Insect Vectors, Institut Pasteur, Paris, France

[3]Veterinary Diagnostic Services, Veterinary School, University of Glasgow, Garscube Estate, Glasgow, United Kingdom, G61 1QH

[4]Institute of Infection, Immunology and Inflammation, College of Medical, Veterinary and Life Sciences, Glasgow Biomedical Research Centre, University of Glasgow, Glasgow, United Kingdom, G12 8TA

[5]Human Histopathology and Animal Models Unit, Institut Pasteur, Paris, France

[6]Institut de Recherche pour le Développement, Unité Mixte de Recherche IRD-CIRAD 177, Campus International de Baillarguet, Montpellier, France

[7]University of Kinshasa, Kinshasa, Democratic Republic of the Congo

[8]Department of Parasitology, National Institute of Biomedical Research (INRB), Kinshasa, Democratic Republic of the Congo

* Joint first authors

** Joint last authors

The authors have no competing financial interests.

Keywords

Skin, blood, reservoir, transmission, infection, Human African Trypanosomiasis, trypanosomes, *Trypanosoma brucei*, tsetse fly, vector-borne, evolution

Abstract

The role of mammalian skin in harbouring and transmitting arthropod-borne protozoan parasites has been overlooked for decades as these pathogens have been regarded primarily as blood-dwelling organisms. Intriguingly, infections with low or undetected blood parasites are common, particularly in the case of Human African Trypanosomiasis caused by *Trypanosoma brucei gambiense*. We hypothesise, therefore, the skin represents an anatomic reservoir of infection. Here we definitively show that substantial quantities of trypanosomes exist within the skin following experimental infection, which can be transmitted to the tsetse vector, even in the absence of detectable parasitaemia. Importantly, we demonstrate the presence of extravascular parasites in human skin biopsies from undiagnosed individuals. The identification of this novel reservoir requires a re-evaluation of current diagnostic methods and control policies. More broadly, our results indicate that transmission is a key evolutionary force driving parasite extravasation that could further result in tissue invasion-dependent pathology.

Introduction

Understanding the process of parasite transmission is essential for the design of rational control measures to break the disease cycle and requires the identification of all reservoirs of infection. In a number of vector-borne diseases, it is becoming evident that asymptomatic individuals, be they humans or animals, can represent a significant proportion of the infected population and therefore an important reservoir of disease that requires targeting by control measures[1-4]. The recent identification in West Africa of asymptomatic individuals with human trypanosomiasis (long-term seropositives) but undetected parasitaemia, raises the question of what role these individuals play in disease transmission[3,5-7]. Therapy is currently only directed towards microscopy-positive individuals and thus a proportion of the infected population remain untreated.

There is convincing evidence that seropositive individuals with low or undetected parasitaemia contain transmissible trypanosomes. Xenodiagnosis experiments, in which tsetse flies are fed on microscopy-negative infected humans[8] or, more recently, experimentally-infected pigs[9], have shown that these apparently aparasitaemic hosts contain the parasite since the tsetse flies became infected. It is uncertain where the trypanosomes reside in the host but, given the telmophagus (slash and suck) feeding habit of the tsetse fly, they could be skin-dwelling parasites ingested with the blood meal. Our findings suggest that parasites may be sufficiently abundant in the skin to allow transmission and therefore the skin may represent an anatomical reservoir of infection.

Detection of trypanosomes in the skin is not well documented, although there are descriptions of cutaneous symptoms associated with African trypanosomiasis and distinct 'trypanid' skin lesions[10]. Imaging data from mouse models of infection suggest that trypanosomes sequester to major organs such as the spleen, liver and brain[11,12] and recent evidence has demonstrated trypanosomes in extravascular adipose tissue[13]. These adipose-associated trypanosomes appear to be a new life-cycle stage with a distinct transcriptional profile and, while tsetse bite-site associated transmission has been suggested[14], and a historical study made a passing observation of localised deposition of trypanosomes in the skin matrix[15], the broader role of skin-dwelling trypanosomes in transmission remains unclear. In this paper we report the investigation of a possible anatomical reservoir in the skin of the mammalian host. We provide conclusive evidence of *T.b. brucei,* (a causative agent of animal trypanosomiasis) and the human-infective trypanosome, *T.b. gambiense,* invading the extravascular tissue of the skin (including but not restricted to the adipose tissue) and undergoing onward transmission despite undetected vascular parasitaemia. We also provide evidence of localisation of trypanosomes within the skin of undiagnosed humans. The presence of a significant transmissible population of *T. brucei* in this anatomical compartment is likely to impact future control and elimination strategies for both animal and human trypanosomiases.

Results

In order to investigate the potential for extravascular skin invasion by *T. brucei*, BALB/c mice were inoculated via IP injection with the low virulence STIB247 strain of *T. brucei* and skin sections were assessed over a 36-day time-course. The presence and relative quantities of extravascular parasites were evaluated by semi-quantitative scoring of the histological samples (Figure 1-source data 1) and compared to blood parasitaemia (Figure 1-source data 2). Extravascular parasites were first observed in the skin 12 days post-infection and remained throughout the experiment. Skin parasite numbers fluctuated to a lesser extent than blood parasitaemia and the apparent periodicity in the skin may be due to one particularly high data point on day 24 (Figure 1). Parasites were found in the dermis, subcutaneous adipose tissue (Figure 2) and in fascia beneath the panniculus carnosus muscle. We did not detect any particular clustering around dermal adipocytes. The presence of parasites in the skin was not associated with major inflammation (Supplementary File 1). To confirm that skin invasion by this parasite was not strain or sub-species specific, the more virulent TREU927 strain of *T. brucei* and the human-infective *T.b. gambiense* strain, PA, were used to infect mice. Extravascular skin invasion of the dermis, subcutaneous adipose tissue and fascial planes (Figure 2-figure supplement 1) was evident with associated mild to moderate inflammation (Supplementary File 2), in some instances the degree of skin invasion in the *T.b. gambiense* infected mice was far greater than *T.b. brucei*, perhaps suggesting a greater propensity for sequestration in this sub-species.

To confirm that the extravascular distribution of parasites was not an artefact of the route of inoculation, infections by natural vector transmission were carried out using a bioluminescent *T.b. brucei* strain, AnTat1.1E AMLuc/tdTomato. Mice were infected by a single infective bite of an individual *G.m. morsitans*. After 4 to 11 days and up to the end of the experiment, parasites were observed in the skin with a dynamic distribution (Figure 3A) and a variable density (Figure 3B). Parasites were first detected in the blood between 5 and 19 days after natural transmission and parasitaemia remained lower than 10^7 parasites/ml. Observed bioluminescence directly reflects the total number of living parasites in the entire organism, including blood and viscera, but the intensity of the signal decreases with tissue depth. Therefore, at the end of each experiment, mice were sacrificed and their organs were checked for bioluminescence. The presence of extravascular parasites in cutaneous and subcutaneous tissues was first demonstrated by bioluminescence imaging in entire dissected skins (Figure 3C) and was not necessarily localised to the bite site. In addition to the skin, only the spleen, some lymph nodes and adipose tissue were observed to be positive for bioluminescence in several individuals (Figure 3-figure supplement 1). This suggests that the observed bioluminescence is likely to originate predominantly, but not solely, from parasites in the skin. In addition, only mild inflammation was observed after 29 days (Figure 3-figure supplement 2).

To confirm that trypanosomes in the skin are a viable population, fluorescent parasites were monitored by two intravital imaging methods following IP injection and natural transmission (Figure 4). First, IP-injected fluorescent *T. brucei* STIB247 were imaged *in vivo* using 2-photon microscopy (Figure 4A). Extravascular trypanosomes observed in the dermal layer of dorsal skin were highly motile, consistent with viability (Video 1). Second, naturally-transmitted fluorescent *T. brucei* AnTat1.1E AMLuc/tdTomato were imaged *in vivo* using spinning-disk confocal microscopy in the C57BL/6J-Flk1-EGFP mouse line that has green fluorescent endothelial cells in the lymphatic and blood vessels[16] (Figure 4B). Extravascular trypanosomes were observed in the dermal layer of the ear and were highly motile (Videos 2, 3 and 4).

Differentiation of dividing trypanosomes to non-dividing stumpy forms is essential for transmission to the tsetse. Using the relative transcript abundance of the stumpy marker Protein Associated with Differentiation 1 (PAD1)[17] to an endogenous control, Zinc Finger Protein 3 (ZFP3)[18], we estimated that approximately 20% of skin-dwelling parasites were stumpy (Supplementary File 3). To directly determine the proportion of stumpy forms in skin sections, histological staining for PAD1 was also performed (Table 1-source data 4). PAD1-positive cells were observed in variable proportions (from 8 to 80%) in all bioluminescent skin samples examined after IP injection (Supplementary File 4). Following natural transmission, up to 38% of parasites detected using VSG surface markers (Figure 3-figure supplement 3A-B) also expressed PAD1 (Figure 3-figure supplement 3C-D) (n=441 cells from 8 skin sections). In all skin sections, stumpy parasites were homogenously distributed in the dermis and subcutaneous adipose tissues.

We next assessed the ability of skin-dwelling parasites to infect tsetse flies. Teneral flies (immature flies that have not yet taken a blood meal) were fed on different regions of skin from mice infected with AnTat1.1E AMLuc/TY1/tdTomato with differing levels of bioluminescence across the skin (Table 1-source data 1 and Table 1-source data 2). This was repeated in 20 mice with differing levels of parasitaemia. Flies were dissected and checked for the presence of fluorescent trypanosomes after two days (Table 1). In mice with undetectable or low parasitaemia ($<5x10^4$ parasites/ml), no parasites were found in flies fed on non-bioluminescent regions. Conversely, a median of 36% (±23%, n=70) of flies that fed on bioluminescent regions of low parasitaemic mice became infected (Table 1 and Table 1-source data 3). This demonstrates that skin parasites, from mice without visible parasitaemia, can contribute to tsetse infection, possibly reflecting human asymptomatic infections. When parasites were detected in the blood and skin, tsetse infection rates increased up to 100% (median of 61% ±22%, n=120) (Table 1 and Table 1-source data 3). Parasites taken-up from the skin were able to further develop through the life-cycle to early procyclic forms in the fly as evidenced by GPEET-procyclin marker on the parasites surface (n=721 cells from 16 flies) (Table 1-source data 4 and Supplementary File 4).

To demonstrate that skin invasion by trypanosomes can occur in humans as well as the murine model, slides of historical skin biopsies, taken as part of a diagnostic screening programme for

Onchocerca microfilaria in the trypanosomiasis-endemic Democratic Republic of the Congo, were examined for trypanosomes. At the time of sampling, the incidence of trypanosomiasis was 1.5-2% and we hypothesised that some individuals may have harboured undiagnosed infections. Re-examination of 1,121 skin biopsies by microscopy revealed six individuals with trypanosomes in their skin (Figure 5). These individuals had not previously been diagnosed with human trypanosomiasis by clinical signs or the presence of blood parasites.

Discussion

We have shown that there exists a significant yet overlooked population of live, motile, extravascular *T. brucei* in the dermis and subcutis of animal models infected by artificial routes or by vector transmission. It is likely that once injected the parasites disseminate via the lymph and blood to the skin where they are ingested during tsetse fly pool-feeding and readily initiate cyclical development in the vector. Given the relative volume of the skin organ compared to the vasculature, it is possible, depending on the density of skin invasion, that more parasites exist in the skin than in the blood. The skin, therefore, represents an unappreciated reservoir of infection. The extravasation of trypanosomes was described previously in major organs such as liver, spleen[11,12] and visceral adipose tissue[13], but the importance of these parasites in transmission was not investigated. Here we show that these skin-dwelling trypanosomes contribute to transmission and could explain the maintenance of disease foci, despite active screening and treatment. Skin invasion for enhanced transmission is likely a powerful evolutionary force driving extravasation, suggesting that the generalised tissue penetration underlying pathogenesis (i.e. splenomegaly, hepatomegaly, CNS invasion) is a secondary epiphenomenon. A skin reservoir also presents a novel target for diagnostics (e.g. skin biopsies), allowing the prevalence of infection to be accurately determined and the identification of any previously undetected animal reservoirs of human disease.

The skin as an anatomical reservoir of parasites is a recurring theme in arthropod-borne human diseases such as *Leishmania*[19,20] and *Onchocerca*[21,22]. Here we present evidence of trypanosomes in the skin of hitherto undiagnosed individuals. This anatomical reservoir may serve to explain how HAT foci re-emerge and persist despite low numbers of reported cases even in the absence of an animal reservoir[23-25].

HAT was once widespread across much of sub-Saharan Africa but concerted control efforts brought it close to elimination during the 1960s[26,27]. However, disease foci persisted, with a resurgence in the number of reported cases to over 300,000 in the 1990s[26-28]. Currently, HAT is approaching elimination in many areas[27,29]. Understanding how HAT evaded elimination in the latter half of the 20th century and how it continues to persist is vital to efforts to eliminate the disease. For example, our results indicate that it may be necessary to develop novel therapeutics capable of accessing extravascular compartments. The current policy in most endemic countries is not to treat serologically positive individuals unless they demonstrate active infection, due to the long duration

and high toxicity of treatment and the low predictive value of the serological tests. We suggest that this policy should be reconsidered in light of our compelling evidence that they represent a carrier population which may maintain HAT foci and explain previously thwarted efforts to eliminate this major pathogen.

Acknowledgments

We acknowledge P. Solano, D. Engman, K. Matthews, M. Taylor, M. Carrington, R. Amino, E. Myburgh and K. Gull for providing various material, cell lines, antibodies and plasmids and to A. Tait for critically reviewing this manuscript.

References

1. Lindblade, K. A., Steinhardt, L., Samuels, A., Kachur, S. P. & Slutsker, L. The silent threat: asymptomatic parasitemia and malaria transmission. *Expert Review of Anti-infective Therapy* **11,** 623–639 (2014).
2. Fakhar, M. *et al.* Asymptomatic human carriers of *Leishmania infantum*: possible reservoirs for Mediterranean visceral leishmaniasis in southern Iran. *Annals of Tropical Medicine & Parasitology* **102,** 577–583 (2013).
3. Koffi, M. *et al.* Aparasitemic serological suspects in *T. b. gambiense* human African trypanosomiasis: A potential human reservoir of parasites? *Acta Tropica* **98,** 183–188 (2006).
4. Berthier, D. *et al.* Tolerance to Trypanosomatids: A Threat, or a Key for Disease Elimination? *Trends in Parasitology* **32,** 157–168 (2016).
5. Jamonneau, V. *et al.* Untreated human infections by *Trypanosoma brucei gambiense* are not 100% fatal. *PLoS Neglected Tropical Diseases* **6,** e1691 (2012).
6. Bucheton, B., MacLeod, A. & Jamonneau, V. Human host determinants influencing the outcome of *Trypanosoma brucei gambiense* infections. *Parasite Immunol.* **33,** 438–447 (2011).
7. Kanmogne, G. D., Asonganyi, T. & Gibson, W. C. Detection of *T. brucei gambiense*, in serologically positive but aparasitaemic sleeping-sickness suspects in Cameroon, by PCR. *Ann Trop Med Parasitol* **90,** 475–483 (1996).
8. Frezil, J. L. [Application of xenodiagnosis in the detection of *T. gambiense* trypanosomiasis in immunologically suspect patients]. *Bull Soc Pathol Exot Filiales* **64,** 871–878 (1971).
9. Wombou Toukam, C. M., Solano, P., Bengaly, Z., Jamonneau, V. & Bucheton, B. Experimental evaluation of xenodiagnosis to detect trypanosomes at low parasitaemia levels in infected hosts. *Parasite* **18,** 295–302 (2011).
10. McGovern, T. W. *et al.* Cutaneous manifestations of African trypanosomiasis. *Arch Dermatol* **131,** 1178–1182 (1995).
11. Blum, J. A., Zellweger, M. J., Burri, C. & Hatz, C. Cardiac involvement in African and American trypanosomiasis. *Lancet Infect Dis* **8,** 631–641 (2008).
12. Kennedy, P. G. E. Human African trypanosomiasis of the CNS: current issues and challenges. *Journal of Clinical Investigation* **113,** 496–504 (2004).
13. Trindade, S. *et al. Trypanosoma brucei* parasites occupy and functionally adapt to the adipose tissue in mice. *Cell Host & Microbe* (2016).
14. Caljon, G. *et al.* The Dermis as a Delivery Site of *Trypanosoma brucei* for Tsetse Flies. *PLoS Pathogens* **12,** e1005744 (2016).
15. Goodwin, L. G. Pathological effects of *Trypanosoma brucei* on small blood vessels in rabbit ear-chambers. *Trans. R. Soc. Trop. Med. Hyg.* **65,** 82–88 (1971).
16. Ema, M., Takahashi, S. & Rossant, J. Deletion of the selection cassette, but not cis-acting elements, in targeted Flk1-lacZ allele reveals *Flk1* expression in multipotent mesodermal

progenitors. *Blood* **107,** 111–117 (2006).
17. Dean, S., Marchetti, R., Kirk, K. & Matthews, K. R. A surface transporter family conveys the trypanosome differentiation signal. *Nature* **459,** 213–217 (2009).
18. Walrad, P., Paterou, A., Acosta-Serrano, A. & Matthews, K. R. Differential Trypanosome Surface Coat Regulation by a CCCH Protein That Co-Associates with procyclin mRNA cis - Elements. *PLoS Pathogens* **5,** e1000317 (2009).
19. Sacks, D. in *Leishmania After the Genome* (2008).
20. Schlein, Y. *Leishmania* and sandflies: interactions in the life cycle and transmission. *Parasitol. Today (Regul. Ed.)* (1993). doi:10.1016/0169-4758(93)90070-V
21. Onchocerciasis. Symptomatology, pathology, diagnosis. (1974).
22. Dalmat, H. T. in *Onchocerciasis* 425 (1955).
23. Kagbadouno, M. S. *et al.* Epidemiology of sleeping sickness in Boffa (Guinea): where are the trypanosomes? *PLoS Neglected Tropical Diseases* **6,** e1949 (2012).
24. Cordon-Obras, C. *et al. Trypanosoma brucei gambiense* in domestic livestock of Kogo and Mbini foci (Equatorial Guinea). *Tropical Medicine and International Health* **14,** 535–541 (2009).
25. Balyeidhusa, A. S. P., Kironde, F. A. S. & Enyaru, J. C. K. Apparent lack of a domestic animal reservoir in *Gambiense* sleeping sickness in northwest Uganda. *Veterinary Parasitology* **187,** 157–167 (2012).
26. World Health Organization. Dept. of Epidemic, Alert, P.Response. WHO report on global surveillance of epidemic-prone infectious diseases. (2000).
27. World Health Organization. Control and surveillance of human African trypanosomiasis. *World Health Organ Tech Rep Ser* 1–237 (2013).
28. Steverding, D. The history of African trypanosomiasis. *Parasites Vectors* **1,** 3 (2008).
29. Simarro, P. P. *et al.* Estimating and Mapping the Population at Risk of Sleeping Sickness. *PLoS Neglected Tropical Diseases* **6,** e1859 (2012).
30. Geigy, R., Kauffmann, M. & Jenni, L. Wild mammals as reservoirs for Rhodesian sleeping sickness in the Serengeti, 1970-71. *Trans. R. Soc. Trop. Med. Hyg.* **67,** 284–286 (1973).
31. Goedbloed, E. *et al.* Serological studies of trypanosomiasis in East Africa. II. Comparisons of antigenic types of *Trypanosoma brucei* subgroup organisms isolated from wild tsetse flies. *Ann Trop Med Parasitol* **67,** 31–43 (1973).
32. Tait, A., Babiker, E. A. & Le Ray, D. Enzyme variation in *Trypanosoma brucei* ssp. I Evidence for the sub-speciation of *Trypanosoma brucei gambiense*. *Parasitology* **89,** 311–326 (1984).
33. Myburgh, E. *et al.* In vivo imaging of trypanosome-brain interactions and development of a rapid screening test for drugs against CNS stage trypanosomiasis. *PLoS Neglected Tropical Diseases* **7,** e2384 (2013).
34. Le Ray, D., Barry, J. D., Easton, C. & Vickerman, K. First tsetse fly transmission of the 'AnTat' serodeme of *Trypanosoma brucei*. *Ann Soc Belg Med Trop* (1977).
35. Xong, H. V. *et al.* A VSG expression site-associated gene confers resistance to human serum in *Trypanosoma rhodesiense*. *Cell* **95,** 839–846 (1998).
36. Fragoso, C. M. & Roditi, I. Highly efficient stable transformation of bloodstream forms of Trypanosoma brucei. *Mol Biochem Parasitol* **153,** 220–223 (2007).
37. Branchini, B. R., Southworth, T. L., Khattak, N. F., Michelini, E. & Roda, A. Red- and green-emitting firefly luciferase mutants for bioluminescent reporter applications. *Anal. Biochem.* **345,** 140–148 (2005).
38. Bastin, P., Bagherzadeh, Z., Matthews, K. R. & Gull, K. A novel epitope tag system to study protein targeting and organelle biogenesis in *Trypanosoma brucei*. *Mol Biochem Parasitol* **77,** 235–239 (1996).
39. Magez, S. & Caljon, G. Mouse models for pathogenic African trypanosomes: unravelling the immunology of host-parasite-vector interactions. *Parasite Immunol.* **33,** 423–429 (2011).
40. Lumsden, W. H. Quantitative methods in the study of trypanosomes and their applications: With special reference to diagnosis. *Bull. World Health Organ.* **28,** 745–752 (1963).
41. Rotureau, B., Subota, I., Buisson, J. & Bastin, P. A new asymmetric division contributes to the continuous production of infective trypanosomes in the tsetse fly. *Development* **139,** 1842–1850 (2012).

42. MacGregor, P., Savill, N. J., Hall, D. & Matthews, K. R. Transmission Stages Dominate Trypanosome Within-Host Dynamics during Chronic Infections. *Cell Host & Microbe* **9,** 310–318 (2011).
43. Zamze, S. E., Ferguson, M. A., Collins, R., Dwek, R. A. & Rademacher, T. W. Characterization of the cross-reacting determinant (CRD) of the glycosyl-phosphatidylinositol membrane anchor of *Trypanosoma brucei* variant surface glycoprotein. *Eur. J. Biochem.* **176,** 527–534 (1988).
44. Kohl, L., Sherwin, T. & Gull, K. Assembly of the paraflagellar rod and the flagellum attachment zone complex during the *Trypanosoma brucei* cell cycle. *J. Eukaryot. Microbiol.* **46,** 105–109 (1999).
45. Makenga Bof, J. C. *et al.* Onchocerciasis control in the Democratic Republic of Congo (DRC): challenges in a post-war environment. *Tropical Medicine and International Health* **20,** 48–62 (2015).

Methods

Trypanosome strains and cultures

All strains used in this study are pleomorphic. STIB247 is a low virulence *T.b. brucei* strain that induces a chronic infection and was isolated from a hartebeest in the Serengeti in 1971[30]. TREU927 is the genome reference strain for *T. brucei* and is more virulent than STIB247. This strain was isolated from a tsetse fly in Kenya in 1969/1970[31]. PA is a human-infective group 1 *T.b. gambiense* strain isolated from a patient in the Democratic Republic of the Congo in 1975[32]. mCherry STIB247 was created by transfection of STIB247 with pHD1034-mCherry[33]. This strain constitutively expresses fluorescent mCherry from the ribosomal RNA promoter and its expression is stable over repeated passage.

The AnTat 1.1E clone of *T.b. brucei* was derived from a strain originally isolated from a bushbuck in Uganda in 1966[34]. Bloodstream forms were cultivated in HMI11 medium supplemented with 10% foetal calf serum at 37°C in 5% CO_2. This strain was genetically engineered to produce two strains continuously expressing the red-shifted luciferase (PpyRE9H) and the tdTomato red fluorescent protein either individually or in combination.

For the first AnTat 1.1E strain, the pTbAMLuc plasmid (M. Taylor, London School of Hygiene and Tropical Medicine, UK) was used for continuous cytosolic expression of the red-shifted luciferase PpyRE9H. The tdTomato coding sequence was cloned with *Hin*dIII and *Bam*HI into the pTSARib vector[35], generating the final pTSARib-tdTomato construct. The two plasmids were linearised with *Kpn*I and *Sph*I restriction enzymes, respectively, and used to transform procyclic parasites with an Amaxa Nucleofector (Lonza)[36]. After 24h, transfected cells were selected by the addition of blasticidin or puromycin (10µg/ml). After one week, the population was examined (i) for red fluorescence by fluorescence microscopy and (ii) for both red fluorescence and bioluminescence by using a fluorimeter Infinite® 200 (Tecan). Cells were sub-cloned by limiting dilution, and clone selection was performed after 15 days by measuring both bioluminescence in a microplate reader

Infinite® 200 (Tecan) and fluorescence with a Muse® cell Analyzer (Merck-Millipore). This strain, named AnTat1.1E AMLuc/tdTomato, was used for natural transmission experiments.

The second AnTat 1.1E strain expressing the 3.1 Kb chimeric multiplex reporter protein PpyRE9H::TY1::tdTomato was named AnTat 1.1E AMLuc/TY1/tdTomato. This cytoplasmic reporter is composed of three distinct markers: the red-shifted luciferase (PpyRE9H) is fused to the tdTomato red fluorescent protein by a TY1 tag. Briefly, the 1.68 Kb optimised version of the North American firefly *Photinus pyralis* luciferase[37] was fused with a 10-bp sequence known as TY1-tag[38] and cloned into the pTSARib plasmid[35] by using *Xho*I and *Hin*dIII restriction enzymes to obtain the pTSARib-PpyRE9H-TY1 plasmid. Finally, the 1.4 Kb coding region of the tdTomato fluorescent protein was inserted downstream using *Hin*dIII and *Bam*HI. The resulting 8.9 Kb vector, containing a blasticidin S resistance cassette, was linearised with *Sph*I to integrate the rDNA promoter locus. Bloodstream parasites were transformed with an Amaxa Nucleofector (Lonza)[36], sub-cloned by limiting dilution, and clone selection was performed by measuring both bioluminescence in a microplate reader Infinite® 200 (Tecan) and fluorescence with a Muse® cell Analyzer (Merck-Millipore). The selected AnTat 1.1E AMLuc/TY1/tdTomato sub-clone was comparable to the parental wild-type strain in terms of growth rate (Table 1-source data 1A), pleomorphism (Table 1-source data 4C), tsetse infectivity and virulence in mice (Table 1-source data 2). In order to verify the reliability of the bioluminescent marker as well as to define the bioluminescence detection threshold of the AnTat 1.1E AMLuc/TY1/tdTomato selected sub-clone, a parasite density / bioluminescence intensity analysis was performed in 96-micro-well plates with an IVIS® Spectrum imager (Perkin Elmer). Parasite density and bioluminescence intensity were correlated when bioluminescence levels were higher than 10^4 p/s/cm²/sr, corresponding to about 10^3 parasites, allowing estimation of the parasite density from *in vivo* imaging over this threshold (Table 1-source data 1B). This correlation was verified by quantification in a microplate reader Infinite® 200 (Tecan) at the very beginning of the first *in vivo* experiment as well as the end of the last one, demonstrating the stability of the triple reporter expression in the AnTat 1.1E AMLuc/TY1/tdTomato selected sub-clone over time, especially after at least one full *in vivo* parasite cycle in the tsetse fly and the mammalian host (Table 1-source data 1C). This strain was used for xenodiagnosis experiments and quantification of parasite densities.

Mouse strains

BALB/c and C57BL/6J mice were used as models for chronic disease[39]. In addition, to allow for further 3D intravital imaging of the lymphatic and blood systems, C57BL/6J-Flk1-EGFP mice expressing a GFP tagged *Kdr* (*Flk1*) gene encoding the vascular endothelial growth factor receptor 2 (VEGFR-2) were used[16].

Ethical statements

This study was conducted under Home Office and SAPO regulations in the UK and in strict accordance with the recommendations from the Guide for the Care and Use of Laboratory Animals of the European Union (European Directive 2010/63/UE) and the French Government. The protocol was approved by the "Comité d'éthique en expérimentation animale de l'Institut Pasteur" CETEA 89 (Permit number: 2012-0043 and 2016-0017) and undertaken in compliance with Institut Pasteur Biosafety Committee (protocol CHSCT 12.131).

Skin invasion time-course

A total of 36 eight-week old BALB/c mice (Harlan, UK) were inoculated by intra-peritoneal (IP) injection with 10^4 parasites of strain STIB 247. Parasitaemia was assayed on each subsequent day using phase microscopy[40]. Twenty-four uninfected animals served as controls. Every three days for 36 days, three infected animals and two uninfected animals were culled and $2cm^2$ skin samples removed from the dorsum. Skin samples were fixed in 10% neutral buffered formalin prior to histological analysis.

Natural infections using tsetse flies

Tsetse flies (*Glossina morsitans morsitans)* were maintained, infected and dissected at the Institut Pasteur as described previously[41]. Flies were infected with AnTat1.1E AMLuc/tdTomato parasites. Positive flies were selected first by screening the abdominal fluorescence (midgut infection) 15 days after the infective meal, and then by a salivation test (mature salivary gland infection) after one month. Single flies with salivary gland infections were used to infect the abdomen of mice anaesthetised by IP injection of ketamine (Imalgene 1000 at 125mg/kg) and xylazine (Rompun 2% at 12.5mg/kg) and feeding was confirmed by visual observation of the fly abdomen full of blood. Control mice were either not bitten or bitten by uninfected flies. The presence and density of parasites in the blood was determined daily by automated fluorescent cell counting with a Muse cytometer (Merck-Milllipore, detection limit 5.10^2 parasites/ml) or by direct examination under a phase microscope with standardised one-use haemocytometers (Hycor Kova, detection limit 10^4 parasites/ml), according to the manufacturer's recommendations.

Infection for xenodiagnosis

A total of 20 seven-week-old male C57BL/6J Rj mice (Janvier, France) were IP injected with 10^5 AnTat 1.1E AMLuc/TY1/tdTomato bloodstream forms. Parasitaemia was assayed daily by automated fluorescent cell counting with a Muse cytometer (Merck-Millipore, detection limit 5.10^2 parasites/ml) according to the manufacturer's recommendations.

PAD1/ZFP3 relative expression

Three BALB/c were infected with *T.b. brucei* strain TREU927 and culled at day 11. The mice were perfused and a $2cm^2$ region of skin removed from the flank. Skin sections were lysed using a Qiagen Tissuelyzer LT and RNA extracted using a Qiagen RNAeasy kit following the manufacturer's instructions. 100ng of RNA from each sample was reverse-transcribed using an Invitrogen Superscript III RT kit. qPCR was performed on each sample using 5µl of cDNA using a protocol and primers validated previously[42] on an Agilent Technologies Stratagene Mx3005P qPCR machine. The ratio of *PAD1* to *ZFP3*, and hence the proportion of cells transcribing the *PAD1* gene, was estimated using the Agilent Technologies MXPro software.

Xenodiagnosis

Mice were first anaesthetised by IP injection of ketamine (Imalgene 1000 at 125 mg / kg) and xylazine (Rompun 2% at 12.5 mg/kg). Batches of 10 teneral male tsetse flies (from 8 to 24 h post-eclosion) were then placed in 50 ml Falcon tubes closed with a piece of net through which they were allowed to feed directly on mouse skin regions of interest for 10 minutes. The selection of the skin regions for fly feeding was based on mice bioluminescence profiles and parasitaemia. Unfed flies were discarded and fed flies were maintained as previously described. Anaesthetised mice were finally sacrificed by cervical dislocation and their skin was dissected for controlling bioluminescence with an IVIS® Spectrum imager (Perkin Elmer). All the flies were dissected and checked for the presence of trypanosomes either 2 or 14 days after their meal on mouse skin by two entomologists blinded to group assignment and experimental procedures. Dissections were performed as previously described[41], entire midguts were scrutinised by fluorescence microscopy to detect and count living red fluorescent parasites, and positive midguts were further treated for IFA. A total of 420 flies were used in 3 independent xenodiagnosis experiments.

***In vitro* bioluminescence imaging**

To perform the parasite density / bioluminescence intensity assay with AnTat 1.1E AMLuc/TY1/tdTomato bloodstream forms, parasites were counted, centrifuged and resuspended in fresh HMI11 medium at 10.10^6 cells/ml. Then, 100µl (or 10^6 parasites) of this suspension were transferred into black clear-bottom 96-well plates and serial 2-fold dilutions were performed in triplicate adjusting the final volume to 200µl of HMI11 with 300 µg/ml of beetle luciferin (Promega, France). Luciferase activity was quantified after 10 minutes of incubation with a microplate reader Infinite® 200 (Tecan), following the instructions of the Promega Luciferase Assay System. After background removal, results were analysed as mean ±SD of three independent experiments.

In vivo bioluminescence imaging

Infection with bioluminescent parasites was monitored daily by detecting the bioluminescence in whole animals with the IVIS® Spectrum imager (Perkin Elmer). The equipment consists of a cooled charge-coupled camera mounted on a light-tight chamber with a nose cone delivery device to keep the mice anaesthetised during image acquisition with 1.5% isofluorane. D-luciferin potassium salt (Promega) stock solution was prepared in phosphate buffered saline (PBS) at 33.33 mg/ml, filter-sterilised and stored in a -20°C freezer. To produce bioluminescence, mice were inoculated IP with 150 µl of D-luciferin stock solution (250mg/kg). After 10 minutes of incubation to allow substrate dissemination, all mice were anaesthetised in an oxygen-rich induction chamber with 2% isofluorane, and images were acquired by using automatic exposure (30 seconds to 5 minutes) depending on signal intensity. Images were analysed with Living Image software version 4.3.1 (Perkin Elmer). Data were expressed in average radiance (p/s/cm²/sr) corresponding to the total flux of bioluminescent signal according to the selected area (total body of the mouse here). The background noise was removed by subtracting the bioluminescent signal of the control mouse from the infected ones for each acquisition.

2-photon microscopy

Intravital multi-photon microscopy studies were carried out using a Zeiss LSM7 MP system equipped with a tuneable titanium:sapphire solid-state two-photon excitation source (4W, Chameleon Ultra II, Coherent Laser Group) coupled to an Optical Parametric Oscillator (Chameleon Compact OPO; Coherent). Movies were acquired for 10 to 15 minutes with an X:Y pixel resolution of 512 x 512 in 2µm Z increments producing up to 40µm stacks. 3D tracking was performed using Volocity 6.1.1 (Perkin Elmer, Cambridge, UK). Values representing the mean velocity, displacement and meandering index were calculated for each object. Mice were anaesthetised IP using medetomidine (Domitor 0.5mg/kg) and ketamine (50mg/kg) and placed on a heated stage. Following removal of hair with a depilatory cream, dorsal skin was imaged. An intravenous injection of non-targeted quantum dots (Qdot705) (Life Technologies, UK) prior to imaging allowed visualisation of blood vessels.

Spinning-disk confocal microscopy

AnTat1.1E AMLuc/tdTomato parasites were monitored in the ear of *Kdr* (*Flk1*) C57BL/6J Rj mice by spinning-disk confocal microscopy as described previously[41]. Briefly, mice were first anaesthetised by IP injection of ketamine (Imalgene 1000 at 125mg/kg) and xylazine (Rompun 2% at 12.5mg/kg). Mice were wrapped in a heating blanket and placed on an aluminium platform with a central round opening of 21mm in diameter. A coverslip was taped on the central hole and the mouse was positioned so that the ear was lying on this oiled coverslip. Imaging was performed using an UltraView ERS spinning-disk confocal system (Perkin Elmer) with a x40 oil objective (1.3 numerical aperture). Movies were acquired by an EM-CCD camera (Hamamatsu) controlled by the Volocity

473 software (Perkin Elmer) with an exposure time of 500ms for a total of 30 to 120s. Images were
474 analysed using ImageJ 1.48v and its plugin Bio-formats importer (NIH).

475 **Histological and immunohistochemical evaluation of the skin**

476 Paraformaldehyde-fixed skin samples were trimmed and processed into paraffin blocks. Sections
477 were stained with Haematoxylin and Eosin (HE). Additional serial sections were processed for
478 immunohistochemical staining using a polyclonal rabbit antibody raised against the invariant surface
479 glycoprotein 65 (IGS65) (M. Carrington, Cambridge, UK) using a Dako Autostainer Link 48 (Dako,
480 Denmark) and were subsequently counterstained with Gill's Haematoxylin.

481 **Histopathological assessment of inflammation in the skin**

482 The extent of cutaneous inflammatory cell infiltration was assessed in haematoxylin and eosin
483 stained sections with a semi-quantitative scoring system applied by two pathologists blinded to
484 group assignment and experimental procedures. The extent of mixed inflammatory cell infiltration in
485 the dermis and/or subcutis was assessed on a 0 to 3 grading scale (0 = no inflammation or only few
486 scattered leukocytes; 1 = low numbers of inflammatory cells; 2 = moderate numbers of inflammatory
487 cells; 3 = large numbers of inflammatory cells). Ten high-power fields were scored for each skin
488 sample. An inflammation score calculated as the average of the scores in the 10 high-power fields
489 was determined for each sample.

490 **Semi-quantitative evaluation of the parasite burden in skin sections**

491 Parasite burden was assessed in skin sections stained with anti-IGS65 antibody by two pathologists
492 blinded to group assignment and experimental procedures. Presence of parasites defined as
493 intravascular (parasites within the lumen of dermal or subcutaneous small to medium-sized vessels)
494 and extravascular (parasites located outside blood vessels, scattered in the connective tissue of the
495 dermis or in the subcutis) was evaluated in 5 randomly selected high-power fields at x40
496 magnification with a 0 to 3 semi-quantitative grading scale (0 = no parasites detectable; 1 = low
497 numbers of parasites (< 20); 2 = moderate numbers of parasites (20 < 50); 3 = large numbers of
498 parasites (> 50). An average parasite burden score was calculated for each sample.

499 **Immunofluorescence analysis**

500 Cells were treated for immunofluorescence after paraformaldehyde or methanol fixation as
501 described previously[17]. Parasites were stained with one or two of the following antibodies: (i) the
502 anti-CRD polyclonal rabbit antibody (1:300) to label the cross-reactive determinant of the
503 glycosylphosphatidylinositol anchors of proteins, predominantly the variant surface glycoproteins[43],
504 (ii) the anti-PAD1 polyclonal rabbit antibody (1:100) targeting the carboxylate-transporter Proteins
505 Associated with Differentiation 1 (PAD1) (Keith Matthews, Edinburgh, UK)[17], (iii) the anti-GPEET
506 mouse IgG3 monoclonal antibody (1:500) targeting the *T. brucei* GPEET-rich procyclin (Acris
507 Antibodies GmbH, San Diego, USA), (iv) the L8C4 mouse IgG1 monoclonal antibody labelling an

epitope of the PFR2 protein[44]. Specific antibodies with minimal cross-reactions with mice and coupled to AlexaFluor 488, Cy3 or Cy5 (Jackson ImmunoResearch, USA) were used as secondary antibodies. DNA was stained with 4,6-diamidino-2-phenylindole (DAPI). IFA image acquisition was carried out on a Leica 4000B microscope with a x100 objective lens using a Hamamatsu ORCA-03G camera controlled by Micro-manager and images were normalised and analysed with ImageJ 1.49v (NIH).

Histopathology of Historical Human Skin Samples

Historical human skin samples were collected from 1991 to 1995 as part of The National Onchocerciasis Task Force (NOTF)[45]. Of this collection, 1,121 paraffin embedded skin samples were cut into 2.5 micron sections and stained with Giemsa (Sigma-Aldrich). Slides were screened for the presence of parasites by two pathologists independently and representative images taken at x100 magnification.

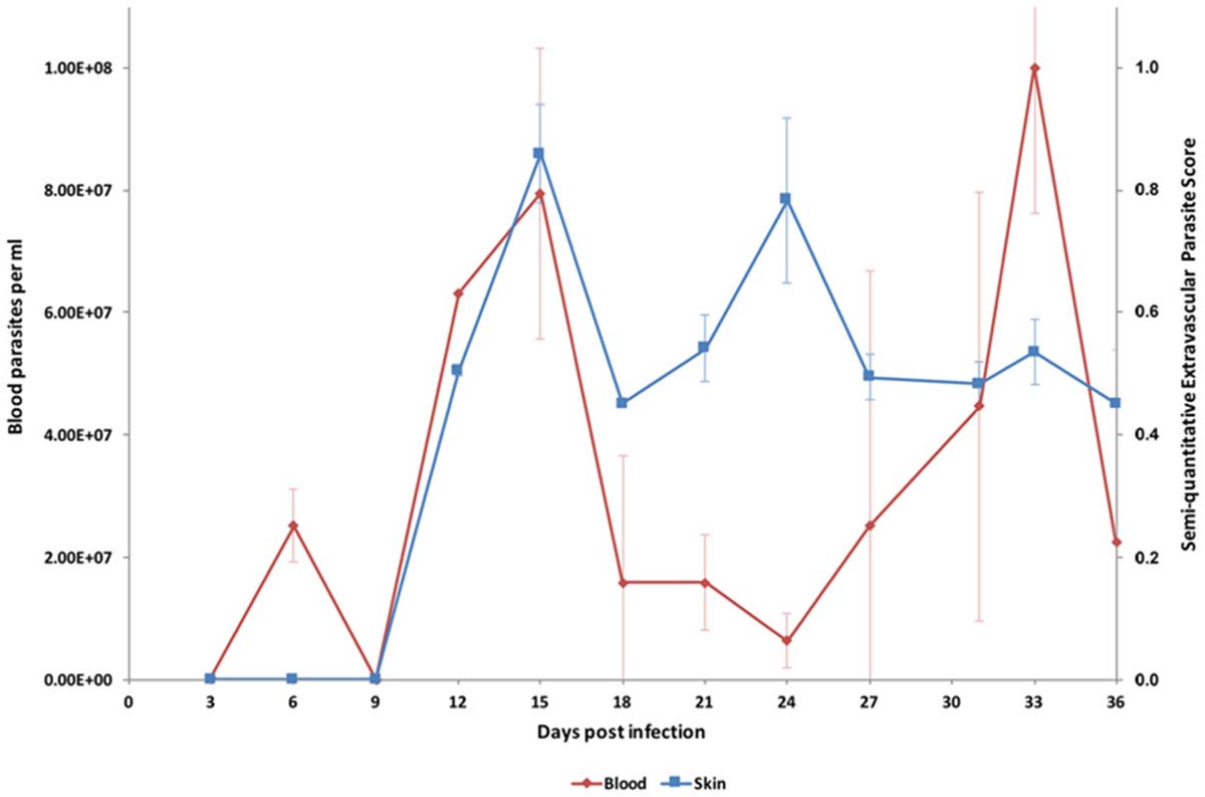

520

521 **Figure 1. Parasite densities in the blood and in the extravascular tissue of the skin over a**
522 **time-course**

523 The blood parasitaemia of *T.b. brucei* strain STIB247 (red) and the semi-quantitative score of
524 extravascular parasites in the skin (blue) are shown over a 36-day time-course following infection in
525 Balb/C mice. Blood parasitaemia was measured using phase microscopy using methodology
526 outlined in [40]. Skin parasite burden is an average of five high-power fields scored by histological
527 analysis (0 = no parasites detectable; 1 = low numbers of parasites; 2 = moderate numbers of
528 parasites; 3 = large numbers of parasites). Standard error shown (n=3).

529

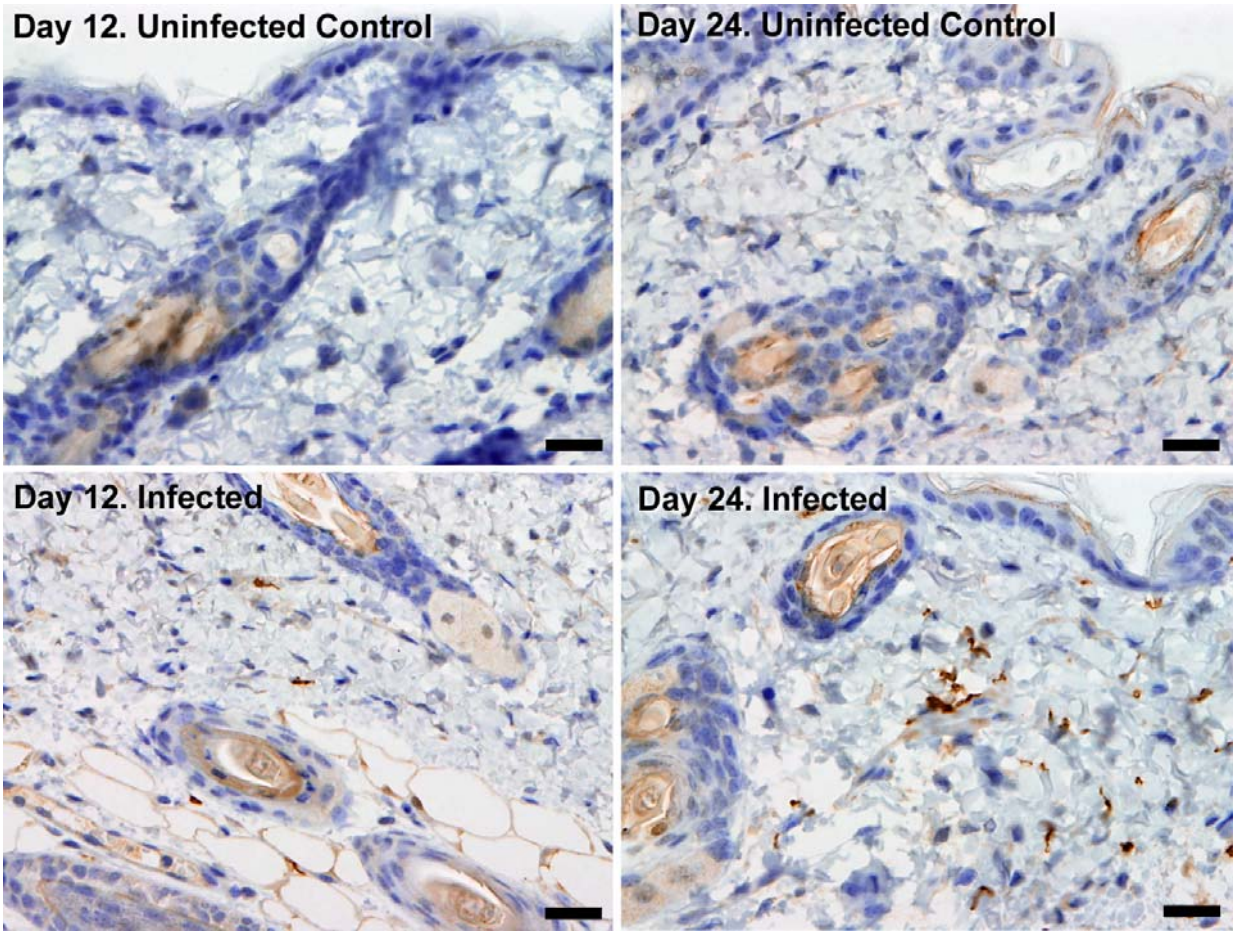

Figure 2. Extravascular localisation of trypanosomes during an infection

Histological sections of dorsal skin from uninfected and infected Balb/C mice stained with trypanosome-specific anti-ISG65 antibody (brown), counterstained with Gill's Haematoxylin stain (blue) at 12 days and 24 days post-inoculation with *T.b. brucei* strain STIB247. Parasites are visible in extravascular locations of the skin including the deep dermis and subcutaneous adipose tissue from day 12. The scale bar represents 20μm.

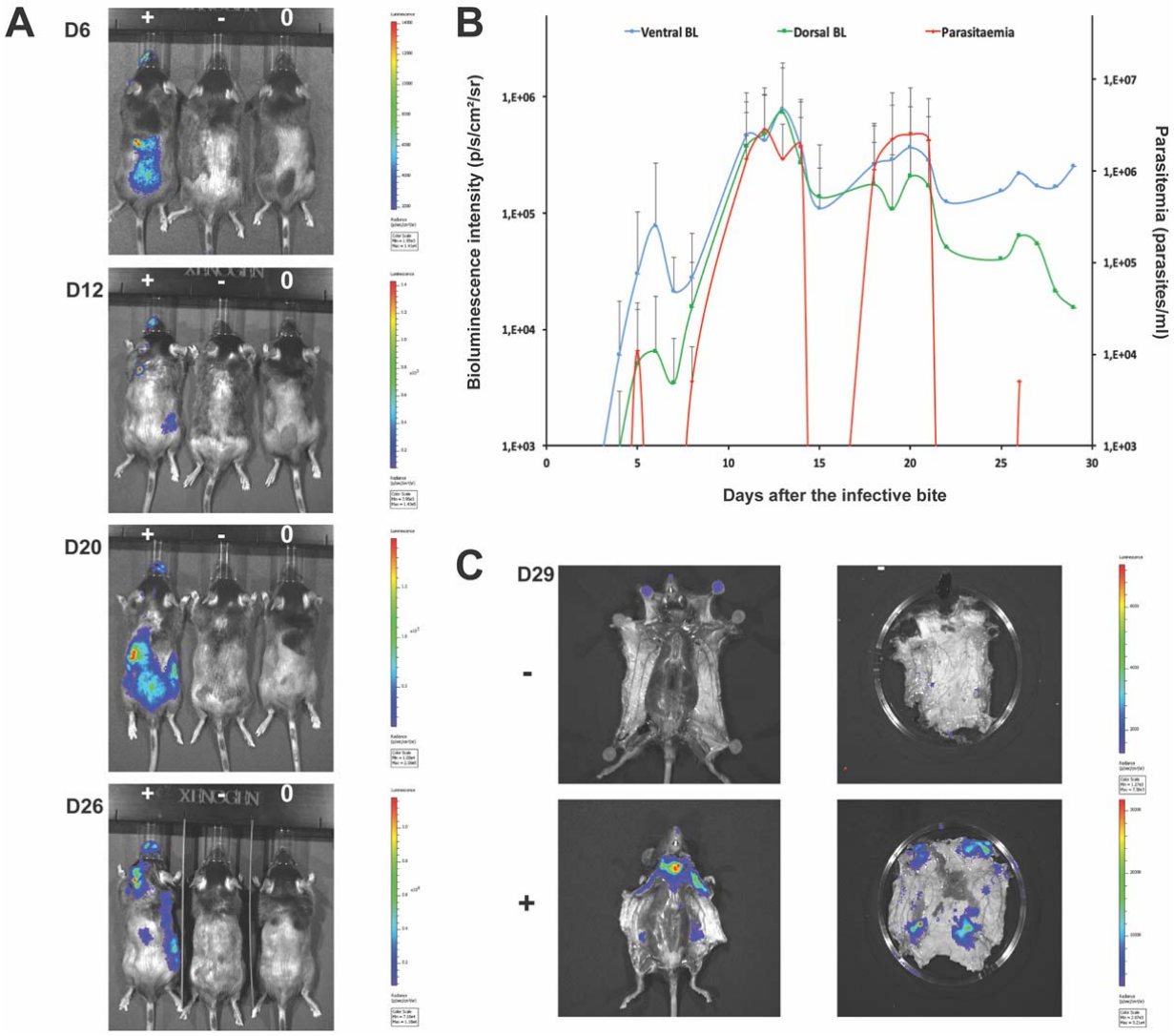

Figure 3. Dynamics of parasite distribution in the extravascular tissue of the skin and in the blood during a representative course of infection following natural transmission

A total of seven mice were infected by the single infective bite of an individual *G.m. morsitans* on the belly with the *T.b. brucei* AnTat1.1E AMLuc/tdTomato strain. Panels A and C depict representative patterns. (A) Examples of bioluminescence profiles of 3 mice (+ bitten by an infected fly, - bitten by an uninfected fly and 0 not bitten) 6, 12, 20 and 26 days after the bite are shown. (B) Ventral (blue) and dorsal (green) bioluminescence (BL) intensities (in p/s/cm^2/sr on the left Y-axis) and parasitaemia (in parasites/ml in red on the right Y-axis) were measured daily for 29 days and plotted as mean ±SD (n=7 mice). (C) The entire skins of mice (+) and (-) were dissected for bioluminescence imaging 29 days after the bite. For the mouse (+), Figure 3–figure supplement 1 shows the bioluminescence profile of dissected organs, Figure 3–figure supplement 2 presents the skin inflammation, and Figure 3–figure supplement 3 shows labelled parasites in skin sections.

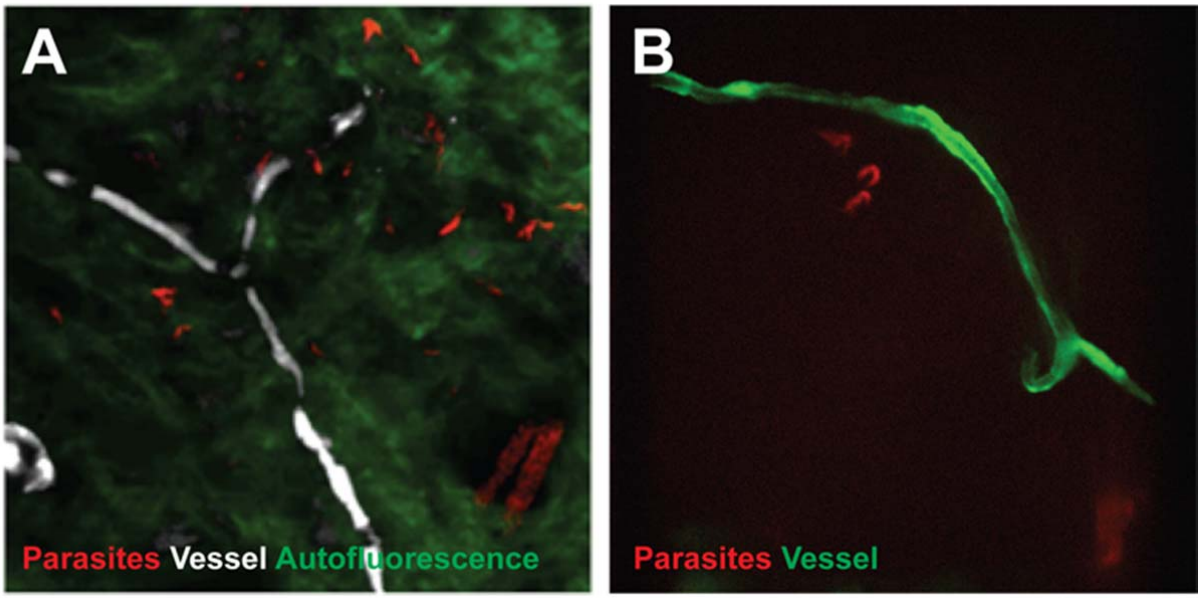

Figure 4. Extravascular localisation of trypanosomes during an infection visualised using multi-photon microscopy (A) and spinning-disk confocal microscopy (B)

(A) Still-image extracted from video (Video 1) of multi-photon live imaging of dorsal skin during a trypanosome infection. Intravenous non-targeted quantum dots (white) highlight blood vessels. *T.b. brucei* STIB 247 parasites transfected with mCherry to aid visualisation (red) are clearly visible and motile outside the vasculature and within the extravascular skin matrix (green). (B) Still-image extracted from (Video 3) of spinning-disk confocal live imaging of the ear of an *Kdr* (*Flk1*) C57BL/6J Rj mouse during a trypanosome infection. *T.b. brucei* AnTat1.1E AMLuc/tdTomato parasites expressing tdTomato (red) are moving in the extravascular region surrounding a vessel of the dermis (green).

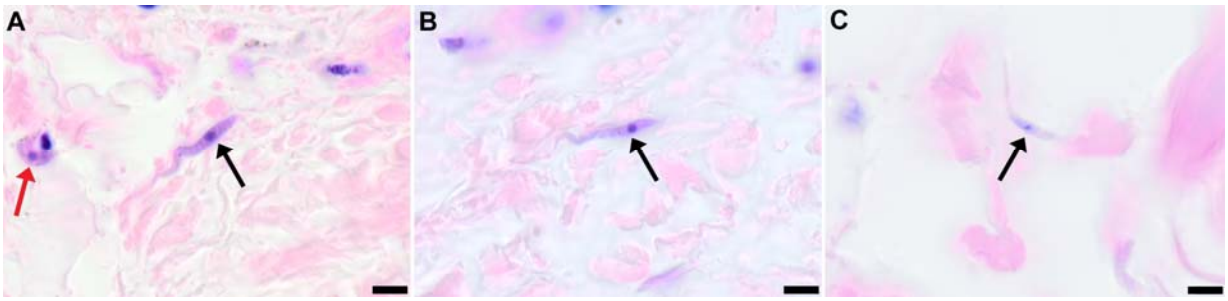

Figure 5. Extravascular localisation of trypanosomes in previously unidentified human cases of trypanosomiasis

Histological sections of skin collected from previously unidentified cases of human trypanosomiasis from the Democratic Republic of Congo, showing the presence of extravascular parasites in biopsies from three individuals (A, B and C). Skin biopsies were collected as part of a national onchocerciasis screening programme that took place in the same geographic region as an active trypanosomiasis focus. Slides were stained with Giemsa and examined under oil immersion at 100x magnification. In addition to visible slender forms (black arrows) in the extravascular tissue of the skin, a clearly identifiable stumpy transmission form with typical morphology and an unattached undulating membrane is also present in the skin of one individual (red arrow in A). The scale bar represents 5μm.

Fly batches	Parasites in blood (per ml)	Parasites in skin (per cm^2)	Dissected flies	Fly infection rates (%)
C1	0	0	32	0%
C	0	0	8	0%
A4B	$< 10^4$	$< 10^3$	16	0%
B1B	$2.2x10^4$	$< 10^3$	13	0%
A4A	$< 10^4$	$6.6x10^5$	17	35%
A2A	$1.1x10^4$	$3.8x10^6$	7	86%
B1A	$2.2x10^4$	$4.6x10^7$	16	31%
3B	$4.4x10^4$	$2.6x10^4$	14	36%
3A	$4.4x10^4$	$2.6x10^4$	16	38%
1B	$1.8x10^5$	$8.0x10^3$	12	67%
1A	$1.8x10^5$	$8.0x10^3$	14	79%
4B	$2.2x10^5$	$1.2x10^4$	17	53%
4A	$2.2x10^5$	$1.2x10^4$	18	56%
2B	$1.6x10^6$	$8.0x10^3$	14	36%
2A	$1.6x10^6$	$3.2x10^4$	18	39%
B4B	$4.3x10^6$	$6.7x10^7$	10	80%
B4A	$4.3x10^6$	$6.7x10^7$	17	100%

Table 1. Skin parasites are ingested during tsetse pool-feeding

Mice were IP infected with *T.b. brucei* AnTat1.1E AMLuc/TY1/tdTomato and the parasitaemia and bioluminescence were monitored daily until the day of xenodiagnosis. The number of parasites in the blood was determined using a haemocytometer or a flux cytometer. The number of parasites in the skin was estimated from the measured bioluminescence intensity by using a standard curve (Table 1-source data 1 and Table 1-source data 2). Batches of teneral flies were fed on different skin regions of mice infected with differing levels of bioluminescence across the skin and with differing levels of parasitaemia (Table 1-source data 2 and Table 1-source data 3). Fly batches A4A, A2A, B1A, 3B and 3A were used to assess tsetse transmission in hosts with low numbers of blood parasites but high numbers skin parasites, while fly batches 1B, 1A, 4B, 4A, 2B, 2A, B2B and B4A were used to investigate the impact of high numbers of parasites in both the skin and blood. Flies were dissected and their midguts checked for the presence of fluorescent trypanosomes after two days to determine the proportion of infected flies (Table 1-source data 4A-B). For some of these experiments, results of an in-depth quantification of parasite stages by IFA is provided in Supplementary file 4. Stumpy forms were observed only in the blood of mice with parasitaemia values highlighted in light grey. Bioluminescence was detected in the skin of mice with values highlighted in dark grey.

Figure Supplements

Figure 2-figure supplement 1. Skin invasion by *T.b. brucei* strain TREU927 and *T.b. gambiense* strain PA

Histological sections of dorsal skin from a mouse infected with *T.b. brucei* strain TREU927 at 20x magnification and two mice infected with *T.b. gambiense* strain PA at 40x magnification 10-days post-inoculation. Trypanosome-specific anti-ISG65 antibody reveals the presence of extravascular parasites (brown) and the slides were counterstained with Gill's Haematoxylin stain (blue) to reveal host skin structure.

Figure 3-figure supplement 1. Bioluminescence mostly originates from parasites in the skin

Mouse (+) was sacrificed and dissected for bioluminescence imaging 29 days after the infective bite. Fig 3C shows the bioluminescence profile of its entire skin and dissected organs are shown here.

Figure 3-figure supplement 2. Mild inflammation of skin tissues one month after an infection by natural transmission

After 29 days, the most bioluminescent skin region of mouse (+) was dissected, fixed in paraformaldehyde, embedded in paraffin and stained with HE. Multifocal inflammatory infiltrates containing neutrophils were located in the dermis and subcutaneous tissue and associated with oedema. Inflammatory foci were generally centred on blood vessels (arrows).

Figure 3-figure supplement 3. Extravascular parasites in the skin express both VSGs and PAD1 surface markers

After 29 days, the most bioluminescent skin region of mouse (+) was dissected, fixed in paraformaldehyde, embedded in paraffin and treated for IFA with the anti-CRD antibody that predominately labels parasites expressing VSGs (A-B), or the anti-PAD1 antibody specific to transmission form "stumpy" cells (C-D).

Source Data

Table 1-source data 1. Characterisation of the AnTat 1.1E AMLuc/TY1/tdTomato sub-clone

(A) The *in vitro* growth of the selected AnTat1.1E AMLuc/TY1/tdTomato sub-clone (red) was similar to that of the parental wild-type strain (blue). Bloodstream forms were cultured in HMI11, counted daily in a Muse cytometer (Merck-Millipore) and diluted after 4 days. (B) A parasite density / bioluminescence intensity analysis was performed by measuring the bioluminescence in successive 2-fold dilutions in 96-micro-well plates with an IVIS® Spectrum imager (Perkin Elmer). When plotted as mean ±SD (n=3), parasite densities and bioluminescence intensities were correlated when the bioluminescence levels were higher than 10^4 p/s/cm²/sr, corresponding to about 10^3 parasites, allowing estimation of the parasite density from *in vivo* imaging over this threshold. This standard curve was used to estimate the number of parasites in the skin from measured values of bioluminescence. (C) This correlation was verified by quantification in a microplate reader Infinite® 200 (Tecan) at the very beginning of the first *in vivo* experiment as well as the end of the last one (mean ±SD, n=3).

Table 1-source data 2. Parasite densities in extravascular tissue of the skin and in the blood of mice used for differential xenodiagnosis

Mice were injected IP with AnTat1.1E AMLuc/TY1/tdTomato and monitored daily for bioluminescence and parasitaemia. (A) Bioluminescence profile of four mice (- uninfected control and (1-3) three infected mice) four days after infection. (B) The entire skins of the uninfected control mouse (-) and mouse 3 were dissected for bioluminescence imaging four days after infection. (C) Parasite densities in the blood and in the skin (calculated from the mean dorsal bioluminescence intensity measurement and from the standard curve in Figure 4-figure supplement 3B, in parasites/cm^2 in blue) were calculated daily over one week and plotted as mean ± SD (n=13 mice).

Table 1-source data 3. Skin parasites are sufficient to initiate a tsetse infection

Schematics summarising the principal results from the xenodiagnosis experiment. In a mouse with no detected transmissible parasites in the blood (absence of stumpy forms by IFA and absence of infection of flies fed on a non-bioluminescent region of the skin), flies can ingest transmissible parasites from the bioluminescent region of the skin (left panel). When a mouse presents transmissible forms in the blood, fly infection rates increase with the concomitant ingestion of parasites from the skin (right panel). Values correspond to those obtained for mouse A4 and B4.

Table 1-source data 4. Parasite stage determination by labelling of specific surface markers

Parasites recovered from infected tsetse midguts (A-B) or included in bloodsmears (C) were fixed in methanol for 5 seconds and stained either with the anti-GPEET antibody detecting early procyclic

forms (red in A-B) and the L8C4 antibody labelling the flagellum PFR (green in A-B), or with the anti-PAD1 antibody detecting intermediate and stumpy forms (green in C), respectively.

Figure 1-source data 1. Semi-quantitative evaluation of the parasite burden in skin sections (STIB247)

Every three days for 36 days of a STIB247 *T.b. brucei* infection, five mice were culled (three infected, two control) and skin sections stained with parasite-specific anti-IGS65 antibody. Parasite burden was assessed by two pathologists blinded to group assignment and experimental procedures. Presence of parasites defined as intravascular (parasites within the lumen of dermal or subcutaneous small to medium-sized vessels) and extravascular (parasites located outside blood vessels, scattered in the connective tissue of the dermis or in the subcutis) was evaluated in 5 high-power fields at x40 magnification with a 0 to 3 semi-quantitative grading scale (0 = no parasites detectable; 1 = low numbers of parasites; 2 = moderate numbers of parasites; 3 = large numbers of parasites).

Figure 1-source data 2. Daily parasitaemia during STIB247 infection in Balb/C mice

The daily parasitaemia during a 36-day STIB247 *T.b. brucei* infection was estimated using phase microscopy and methodology outlined in [40].

Supplementary Files

Supplementary File 1. Histopathological assessment of inflammation in the skin during STIB247 infection

The extent of cutaneous inflammatory cell infiltration during the 36-day STIB247 experiment was assessed on haematoxylin and eosin stained sections with a semi-quantitative scoring system applied by two pathologists blinded to group assignment and experimental procedures. The extent of mixed inflammatory cell infiltration in the dermis and/or subcutis was assessed on a 0 to 3 grading scale (0 = no inflammation or only few scattered leukocytes; 1 = low numbers of inflammatory cells; 2 = moderate numbers of inflammatory cells; 3 = large numbers of inflammatory cells). Ten high-power fields (HPFs) were scored for each skin sample.

Supplementary File 2. Histopathological assessment of inflammation in the skin during TREU927 infection

The extent of cutaneous inflammatory cell infiltration at day 10 of infection by strain TREU927 experiment was assessed on haematoxylin and eosin stained sections with a semi-quantitative scoring system applied by two pathologists blinded to group assignment and experimental procedures. The extent of mixed inflammatory cell infiltration in the dermis and/or subcutis was assessed on a 0 to 3 grading scale (0 = no inflammation or only few scattered leukocytes; 1 = low numbers of inflammatory cells; 2 = moderate numbers of inflammatory cells; 3 = large numbers of inflammatory cells). Ten high-power fields (HPFs) were scored for each skin sample.

Supplementary File 3. Expression of PAD1 relative to ZFP3

The relative abundance stumpy cells in the skin of three BALB/c was estimated using qPCR at day 11 post-inoculation with *T.b. brucei* strain TREU927. Mice were culled and perfused to remove blood parasites and a $2cm^2$ region of skin removed from the flank. The tissue was homogenised and RNA extracted. 100ng of RNA from each sample was reverse-transcribed and qPCR performed to estimate the cycle thresholds (C_T) of the stumpy marker PAD1 and the endogenous control ZFP3. As C_T is inversely proportional to amount of target cDNA in the sample and PAD1 and ZFP3 have similar qPCR efficiencies, a comparison of the delta (Δ) of C_T between PAD1 and ZFP3 transcripts reveals the relative ratio of PAD1 to ZFP3 transcripts and hence the proportion of differentiated parasites transcribing the PAD1 gene.

Supplementary File 4. Both the respective densities and the proportions of transmissible forms of parasites in the skin and in the blood govern the tsetse infection rates during pool feeding

For some of the xenodiagnosis experiments shown in Table 1, identification and quantification of

parasite stages was performed by IFA on blood smears and skin sections. Stumpy forms were observed only in the blood of mice with parasitaemia values highlighted in light grey. Bioluminescence was detected in the skin of mice with values highlighted in dark grey. The number of parasites in the skin was calculated according to the values obtained in the standard *in vitro* assay (Table 1-source data 1) and is therefore probably an underestimate. Tsetse flies were dissected 2 days after xenodiagnosis. Populations of intermediate and stumpy form cells were assessed in blood smears and in successive skin sections stained either with the anti-CRD antibody or the anti-PAD1 antibody (see Method section). Populations of early procyclic cells were assessed in dissected fly midguts stained with the anti-GPEET antibody (see Method section). ND: not determined.

Video 1. Extravascular trypanosomes visualised in the skin using 2-photon microscopy

Intravital multi-photon imaging of the flank skin during trypanosome infection 10 days after IP inoculation. An intravenous injection of non-targeted quantum dots prior to imaging allowed visualisation of blood vessels. mCherry STIB247 *T.b. brucei* parasites (red) are observed moving in the extravascular region surrounding blood vessels of the dermis (white). Collagen auto-fluorescence is visible as green.

Videos 2-4. Extravascular trypanosomes visualised in the skin using spinning-disk confocal microscopy

Spinning-disk confocal live imaging of the ear of an *Kdr* (*Flk1)* C57BL/6J Rj mouse during a trypanosome infection after natural transmission. *T.b. brucei* AnTat1.1E AMLuc/tdTomato parasites expressing tdTomato (red) are observed moving in the extravascular region surrounding blood and / or lymphatic vessels of the dermis (green).